Velocity Field Retrieval from Long Term Coherent Points in Radar Interferometric Stacks

Bert M. Kampes and Nico Adam
German Space Agency, DLR-Oberpfaffenhofen, Germany
Email: bert.kampes@dlr.de

***Abstract*— This paper addresses the question of how to robustly estimate linear deformation at a large number of points from differential phase in an interferometric stack. The so-called "Permanent Scatterers technique" [1], uses a relatively large number of differential interferograms of the same area, co-registered at the same master SLC image. Linear deformation rates and DEM errors are estimated for pixels that have limited temporal decorrelation. This straightforward and generic setup has been used in a network approach that uses connections between nearby points to compute a velocity field for large areas.**

I. Introduction

Using a multi-temporal dataset can overcome the problems of 2D phase unwrapping and atmospheric artifacts in conventional radar interferometry. The loss of spatial coherence due to temporal decorrelation is the main cause of the phase unwrapping problem. A very generic approach using point scatterers time series has been recently introduced that circumvents this problem by only considering pixels that have no temporal decorrelation, "the Permanent Scatterers technique" (PS), see [1]. Since temporal decorrelation results from (random) physical changes of the individual scattering centers within each resolution cell over the time period between observations [2], point scatterers by definition do not suffer from this effect. The PS technique can be applied to data with large perpendicular baselines, even from different sensors with slightly different wavelengths. Applications include convenient and low-cost monitoring of the global deformation pattern of cities, movements of individual buildings caused by infrastructural projects, stability analysis for industrial complexes, as well as monitoring of deformations caused by mining. The most important features of the PS technique are that it enables

- straightforward data handling and processing;
- combination of all available ERS images in the data archive, regardless of perpendicular baseline or Doppler frequency;
- extension of the time series with data of ENVISAT, which operates on a slightly different wavelength;
- computation of (low frequency parts of) the atmospheric phase;
- circumvention of spatial unwrapping in favor of an implicit time wise unwrapping.

The next section describes the differential interferometric SAR processing system, followed by the estimation strategy and application to Berlin, Germany.

II. InSAR processing

The following is a listing of mainly differences with conventional processing to describe how we compute a stack of differential interferograms.

- Image selection: For many areas there is a considerable amount of data available, and if not all images can be bought, a choice needs to be made regarding which data to process. An extremely useful tool for this selection is a baseline plot, which shows the distribution of the images as function of perpendicular and temporal baseline, and of Doppler frequency. We select images, in a (semi-)automated way, that are as equidistant as possible in time, spanning the period of interest. We prefer to select images with limited perpendicular baselines to reduce geometric decorrelation and topographic induced phase.
- Master image selection: A master image is selected on which all other images are co-registered. This image lies centrally in the baseline plot, i.e., in time, space and Doppler frequency. This choice reduces problems during the co-registration. The selection of a master l is automated by computing a total correlation for each possible stack as $\gamma^l = 1/K \sum_{k=0}^{K} c(\mathtt{B}_{\perp}^{\mathtt{k,1}}, 1200) \times c(\mathtt{T}^{k,l}, 5) \times c(\mathtt{f}_{\mathrm{DC}}^{k,l}, 1380)$, where $c(x,\alpha) = 1 - |x|/\alpha$ if $\alpha < x$; 0 otherwise. Note that here the temporal baseline is in years, and that the divisors can be regarded as *critical baselines* for which total decorrelation occurs.
- Amplitude calibration: The amplitude of the SLC images are calibrated for sensor gain, range spreading loss, and antenna pattern. This is performed to be able to analyze the amplitude time series, but it also generates as a by-product a high resolution mean amplitude map, with a high number of looks.
- Data oversampling: The complex data are oversampled by a factor of two in both directions in order to avoid aliasing effects in the interferometric phase.
- Differential interferogram generation: The interferograms are corrected for topographic signal using an external DEM. If available we use the DEMs generated from the X-SAR shuttle mission [3], otherwise a DEM derived from the ERS tandem mission. But any available DEM can be used to reduce the topographic signal.
- Filtering: No spectral or phase filtering is applied during the InSAR processing, since we do not want to affect the phase of the point scatterers selected for analysis.

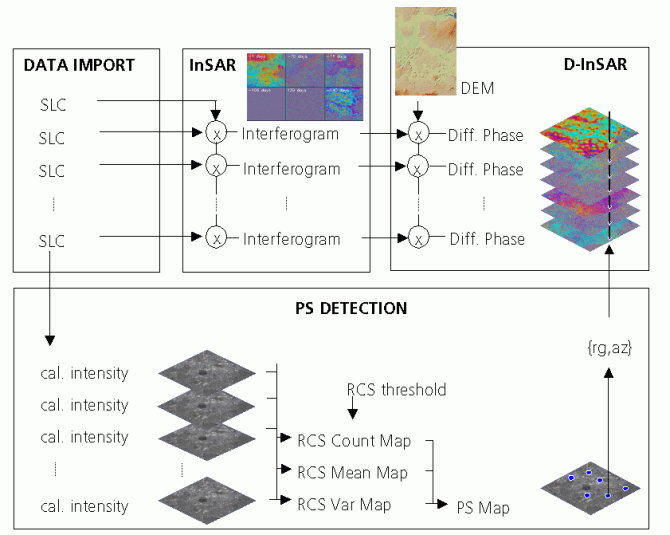

Fig. 1. Data flow for differential interferometric SAR processing and preliminary identification of point scatterers.

Fig. 1 shows the data flow for a "Permanent Scatterers" system, taken from [4]. Input are $K+1$ Single Look Complex images. The amplitude is calibrated and is the basis for the selection of point scatterers, as shown on the lower right. The interferograms are generated and a DEM is used to compute the differential interferograms. Now that we have the interferograms, points have to be selected that are most likely to contain a limited amount of temporal decorrelation.

A. Identification of pixels with limited temporal decorrelation

Note that the phase information itself cannot be used for detection of stable points, since it contains phase induced by unknown elevation and deformation. Ferretti pointed out that the amplitude time series can be well used for this [1]. By far most pixels of the interferograms are not expected to contain useful phase information due to temporal decorrelation. Indeed most interferograms resemble random noise on visual inspection. It is expected, however, that pixels with a relatively large calibrated amplitude a_k in all SLC images $k = 0 \ldots K$, have a relatively small phase standard deviation, and contain useful phase information. The selected pixels fulfill two criteria; the amplitude is above a threshold N_2 in at least N_1 SLC images (2), and the ratio of the standard deviation and mean is above another threshold N_3 (2).

$$\sum_{k=0}^{K} \alpha_k \geq N_1, \quad \alpha_k = \begin{cases} 1, & a_k > N_2 \\ 0, & \text{otherwise} \end{cases} \tag{1}$$

$$\frac{\sigma_a}{\overline{a}} \geq N_3. \tag{2}$$

These thresholds do not have to be extremely selective since in the first step of our algorithm only the best pixels are considered. Analysis of the phase data itself will reveal if the other selected pixels are reliable or not. The pixels that are not selected in this step are discarded in the further processing, since it is not expected that they contain useful phase information.

B. Estimation between pixels

We consider phase differences between nearby points in order to limit the influence of atmospheric delays and orbit errors. The functional relation of the phase difference between points P and Q of the reference phase corrected differential interferogram k with DEM error difference $\mathtt{h}_{\mathrm{P,Q}}$ and deformation rate difference $\mathtt{v}_{\mathrm{P,Q}}$, is given as

$$\phi^k_{\mathrm{P,Q}} = -\frac{4\pi}{\lambda} \frac{\mathtt{B}^{\mathtt{k}}_{\perp_{\mathrm{P}}}}{\mathtt{r}_{\mathrm{P}} \sin\theta_{\mathrm{P}}} \mathtt{h}_{\mathrm{P,Q}} - \frac{4\pi}{\lambda} \mathtt{T}^k \mathtt{v}_{\mathrm{P,Q}} + \phi^l_{\mathrm{ATMO_{P,Q}}}, \tag{3}$$

where the wavelength is denoted by λ, the perpendicular baseline by $\mathtt{B}_\perp$, the slant range by $\mathtt{r}$, and the viewing angle by θ. Note that for a system with multiple wavelengths, the wavelength is that of the slave sensor.

The interferometric atmospheric phase difference at the points is the difference during the acquisitions for master l and slave k, $\phi^k_{\mathrm{ATMO_{P,Q}}} = \phi^l_{\mathrm{ATMO_{P,Q}}} - \phi^k_{\mathrm{ATMO_{P,Q}}}$. In (3) we added the atmospheric phase for the master l, since this is present in all interferograms as a bias in the time series approach. Note that (3) describes a plane in the conversion factors for height to phase and velocity to phase, with the height and velocity as slopes.

The noise on the phase difference is assumed to be Gaussian. The variance of the phase noise of the difference signal is twice that of a single point. The atmospheric signal of the slaves is moved to the noise part. This can be done without problem since the atmospheric states during the acquisitions are unrelated, but fortunately are spatially correlated. The radar signal travels through almost the same part of the atmosphere for nearby pixels, and the phase offset due to water vapor is also practically equal for both pixels. The further the pixels are separated, the less correlated they will be. For distances up to 500 meter the atmospheric difference signal can be regarded below the noise level of the observations, see [5]. The data is assumed to contain no significant trends due to orbit errors. We found it to be necessary to remove these errors in a preprocessing step, however.

From the observed phase time series of the differential interferograms, we would like to infer the elevation difference and deformation rate difference. This is a non-linear problem, since the observed phase is wrapped in the principal interval $[-\pi, \pi\rangle$. Furthermore, the problem is relatively sensitive to noise on the observations due to the non-linearness. There are a number of solutions that are strongly correlated. The more observations, the more distinguishable the correct solution is.

The absolute value of the ensemble coherence γ can be considered as a norm

$$\gamma = \frac{1}{K} \sum_{k=1}^{K} e^{jw_k}, \tag{4}$$

with j the imaginary unit, and w_k the residual between the observed phase difference and the phase modeled according to (3). The angle of the complex coherence is an estimate

for the mean residual phase between the points, i.e., $\phi^{l}_{\mathrm{ATMO}_{P,Q}}$. We estimate $\mathtt{h}_{P,Q}$ and $\mathtt{v}_{P,Q}$ by maximizing the magnitude of the coherence. The algorithm we applied systematically steps through the solution space while evaluating the coherence. If information is available on the quality of the interferograms, for example from analysis of a coherent patch or from meteorological data, it can be used to weight the residues accordingly in (4).

III. Network Algorithm

After the differential interferometry we assume to have a set of pixel positions that are most likely to possess limited temporal decorrelation, or none at all. The differential interferometric phase and calibrated amplitude are known for each interferogram and position, as well as factors to convert phase to height and phase to deformation rate (using the temporal and perpendicular baselines, see (3)).

The idea of our algorithm is to first form a stable reference network between the best points in this set, and thereafter to estimate the parameters for the other points with respect to this network. This enables a quality control and description of the estimated parameters. It can be well compared to the way new points are measured in classical geodesy, where also first a reference network is established, and more points are added later. For example, in a leveling campaign the observations are tied to a national reference network of stable points with known height. Since phase differences between nearby pixels are considered, a large area can be processed, without problems due to atmospheric disturbances.

A. Construction of reference network

To form a reference network, we want to find a set of pixels that are distributed equally over the area of interest, and that have a phase that is induced mainly by elevation and (linear) deformation. Therefore, a grid is placed over the interferogram, and in each grid cell the pixel is selected that has the largest ratio of amplitude standard deviation and mean amplitude (2). To avoid pixels very near to each other, this procedure is repeated with the grid shifted by half the cell width in both directions. This ensures a minimum distance between selected pixels of half the cell width. Typical values for the cell width are in the range of a few hundred meters. Before placing the first grid, points are removed with a very low mean. This procedure does not guarantee that the selected pixels have a linear deformation pattern, of course. But this is not an uncommon assumption, since it is likely that most pixels deform at a constant rate for most applications. Furthermore, the relative deformation of nearby pixels is considered, making it more likely that the difference in deformation is dominantly linear with time. Also, pixels that do not fit in with the other pixels in the reference network are removed in the testing procedure described below. A network is constructed between the pixels selected to serve as reference for the other pixels. This means that pixels in each others proximity are connected via arcs (in its most simple form by Delaunay triangulation), and that the height and velocity rate differences are estimated at these arcs by maximizing the coherence (4).

It is important to note that these estimates are not "independent observations"; the phase difference time series used to estimate the parameters are computed by subtracting the phases at the pixels themselves, and are not observed at the arcs of the network. This means that, for example, if the height differences in a small triangle are considered, the closing error by definition must equal zero. However, a closing error can occur for several reasons. Since we sample the solution space, we may do this too coarsely and miss the global maximum for a certain arc. Also, the signal we are looking for may simply lie outside our search space, and it will alias somewhere in our estimation. Finally, the point we consider may not be a coherent point at all, meaning that all arcs to this point are randomly estimated.

B. Adjustment and testing of reference network

After we have obtained estimates for DEM error, velocity, and atmospheric differences between the points of the reference network, a least squares adjustment is carried out to obtain the values for these parameters at the points. These differences are adjusted separately, much like an ordinary leveling network is adjusted. Because the observations are themselves estimated from the phase time series at the points—and not observed at the arcs—the adjusted residuals should be zero, i.e., there should be no inconsistencies. The goal of the testing step is to identify and remove points and arcs that are not reliable, until a stable solution has been reached.

1) Adjustment: A system of linear equations can be written as

$$\mathsf{E}\{\underline{\mathtt{y}}\} = \mathtt{A}\mathtt{x}; \quad \mathsf{D}\{\underline{\mathtt{y}}\} = \mathtt{Q}_y. \tag{5}$$

The functional model links the observations in vector $\underline{\mathtt{y}}$ $[m\times 1]$ to the unknown parameters $\mathtt{x}$ $[n \times 1]$ via the design matrix $\mathtt{A}$ $[m\times n]$, while the stochastic model describes the dispersion of the observations by the variance-covariance matrix $\mathtt{Q}_y$ $[m\times m]$. In our application this matrix is assumed to be diagonal. The observations contain the differences at the arcs of the network, and the design matrix contains -1 and 1 at the corresponding places. It is the same for all three networks. The least squares solution for the parameters is given by [6]

$$\underline{\mathtt{x}} = (\mathtt{A}^{\mathsf{T}}\mathtt{Q}_y{}^{-1}\mathtt{A})^{-1}\mathtt{A}^{\mathsf{T}}\mathtt{Q}_y{}^{-1}\underline{\mathtt{y}}. \tag{6}$$

The adjusted observations are given by $\underline{\mathtt{y}} = A\underline{\mathtt{x}}$, and the residuals on the observations by $\underline{\mathtt{e}} = \underline{\mathtt{y}} - \underline{\mathtt{y}}$. The least squares estimate ensures a minimum l_2 norm of the adjusted residuals.

Note that in order to obtain a solution, a reference point needs to be chosen. All estimates are relative to this point.

2) Testing: It is good practice in geodesy to always perform statistical tests of the least squares adjustment for model misspecifications and outlier observations ("blunders"). In our case, we perform combined tests for the three networks, since it cannot be the case that, for example, an arc is wrong in the estimated height differences, but not in the velocities.

The most general test that can be performed is called the Overall Model Test (*OMT*). If this test is rejected, it means that either the functional, or the stochastic model contains an error. It is also possible to use alternative hypotheses specifying a gross error in an individual outlier (in all three networks), or for all arcs leading to a point (in all three networks). We refer to these tests as *w-tests* and *p-tests* respectively.

In order to compare these tests of different dimensions, and to identify what is the most likely alternative hypothesis to accept, these tests are normalized by division by their critical values. As power for all tests a value of 0.50 must be chosen. Furthermore, we choose a level of significance for the 1D-test of 0.001. The required a-priori variances for the differences at the arcs are computed from the estimation itself (i.e., from the baseline configuration). Also see [7].

A DIA testing procedure is followed. If the OMT is rejected, and a mis-specification Detected, the most likely cause is Identified by specifying several alternative hypotheses. Finally, the functional model is Adapted for this by removing the concerned observations from the observation vector, design matrix, and possibly vector of unknowns, and then the OMT is computed again. This can be summarized in pseudo-code as

```
while (OMT > 1)//                          Detection
  compute::w-tests;//                 Identification
  compute::p-tests;
  if (max(w-tests)>max(p-tests)
    remove::identified arc;//              Adaption
  else
    remove::identified point;
  compute::LS adjustment reduced system
  compute::OMT quotient
```

C. Estimation w.r.t. reference network

Once the reference network is established, i.e., the elevation and velocity rate of the points in the reference network are computed and tested, the other originally selected points can be estimated with respect to this network. Each new point is connected to a maximum of five nearest points of the reference network within a maximum range (3 km), and the elevation and velocity rate differences at these arcs are estimated in the same manner as for the arcs of the reference network by maximizing of the coherence (4).

After this step, the reliability of the new points can be evaluated by the residues at the arcs to the reference network, or by using the estimated coherence.

IV. Test area Berlin

The algorithm has been applied to analyze the city of Berlin, Germany (frame 2547, track 165). We used 69 SLC images, spanning a time period of 8.5 years. The span of the perpendicular baselines was 2100 meter. The area we computed was approximately 25 by 25 km, and about 200,000 points were identified as possible stable point. The reference network contained 2090 points, with a mean distance at the arcs of 600 m. The estimated linear deformation in the line of sight is shown in Fig. 2. Plotted are about 60,000 points

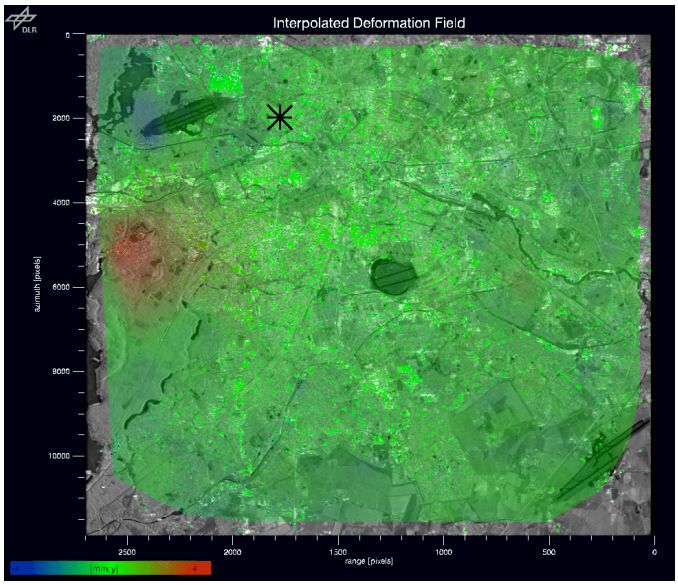

Fig. 2. Estimated linear deformation for Berlin.

with a coherence above 0.70, in the interval $[-4, 4]$ mm/y. The background is the mean calibrated amplitude, and an interpolated velocity is drawn in a transparent layer. The reference point is plotted as an asterisk. It can be observed that deformation is taking place in the west at a rate of a few mm/y. We validated these results by processing a parallel track with the network algorithm. This work is ongoing, but first results are very encouraging.

V. Conclusion

The presented network algorithm for analysis of multi-temporal interferometric data is a robust estimator that can be applied in many cases. The processed area is unlimited in size, as long as point scatterers are within a few kilometers. The suggested testing procedure enables a robust and reliable estimation, also when less data is available then we used in the example provided.

References

[1] A. Ferretti, C. Prati, and F. Rocca, "Permanent scatterers in SAR interferometry," *IEEE Transactions on Geoscience and Remote Sensing*, vol. 39, no. 1, pp. 8–20, Jan. 2001.

[2] H. A. Zebker and J. Villasenor, "Decorrelation in interferometric radar echoes," *IEEE Transactions on Geoscience and Remote Sensing*, vol. 30, no. 5, pp. 950–959, sept 1992.

[3] S. Suchandt, H. Breit, N. Adam, M. Eineder, B. Schättler, H. Runge, A. Roth, and E. Mikusch, "The shuttle radar topography mission," in *ISPRS Workshop, High Resolution Mapping from Space, 19. - 21. September, Hannover, Germany*. ISPRS, Sept. 2001, pp. 235–242.

[4] N. Adam and B. M. Kampes, "Permanent scatterer: Software documentation," 2002, internal technical notes.

[5] R. F. Hanssen, *Radar Interferometry: Data Interpretation and Error Analysis*. Dordrecht: Kluwer Academic Publishers, 2001.

[6] P. J. G. Teunissen, *Adjustment theory; an introduction*, 1st ed. Delft: Delft University Press, 2000.

[7] ——, *Testing theory; an introduction*, 1st ed. Delft: Delft University Press, 2000.